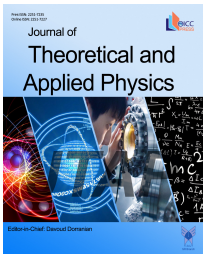

Volume 18, Issue 4, 182449 (1-9)

Journal of Theoretical and Applied Physics (JTAP)

https://dx.doi.org/10.57647/j.jtap.2024.1804.49

Plasma surface interaction for constant mean free path

Rajat Dhawan*, Sarika, Rajeev Sehrawat, Rashmi Mittal, Ishan Choudhary

Department of Physics, MM Engineering College, Maharishi Markandeshwar (Deemed to be University), Mullana-Ambala, Haryana, India.

***Corresponding author:** rajatdhawan147@gmail.com

Original Research

Received:
2 May 2024
Revised:
4 June 2024
Accepted:
9 June 2024
Published online:
30 August 2024

Abstract:

In the present work, plasma surface interaction for constant mean free path has been investigated by choosing a three-component electronegative warm plasma where electrons are described by non-extensive statistics, and both negative and positive ions by fluid approach. Here, the finite value of ion-neutral collisions, the temperature of negative and positive ions, the mass of negative ions, and negative ion density have been considered to uncover the realistic situation. We have considered CF_4 electronegative plasma where CF_3^+ and F^- are the dominant charged species formed. The influence of electronegativity and positive ion temperature on positive ion velocity, positive ion density, electric potential, and net space charge density have been analysed to uncover the realistic situation. The plasma sheath profile has been investigated for the very first time using this combination of charged species distribution.

Keywords: Plasma surface interaction; Plasma sheath; Electronegative plasma; Non-extensive statistics; Constant mean free path; Fluid behaviour

1. Introduction

When a plasma comes into the contact of a surface, a thin layer of charged species called a sheath form near the surface. This happens because plasma's charged particles, like negative ions, positive ions, and electrons, interact with the surface. The whole geometry has been classified into three parts: sheath region, pre-sheath region and bulk plasma region. Sheath region is closest to the surface. Most of the charge particles it contains are the positive ions because they are strongly attracted to the surface. Hence, this region is rich in positive ions density only. Presheath region is next to the sheath region and goes further into the plasma. Here, the positive ions are accelerated towards the surface of the wall/probe by an electric field. This creates a flow of positive ions towards the surface. In bulk plasma region, charged particles exist in approximately equal numbers, which makes the overall charge of the plasma close to neutral.

Depending upon the variety of charged particles available in the plasma, it can be classified into two categories: electropositive plasma and electronegative plasma. Electropositive plasma contains two charged species, namely positive ions and electrons, are present along with the neutral atoms. Electropositive plasmas can be created in different ways such as by using DC discharge, radio-frequency discharge, micro-wave discharge, etc. Electronegative plasma is a special kind of plasma where in addition to positive ions and electrons, third charged species namely negative ions are also present in the plasma system. In order to produce electronegative plasma, we are using gases that have a strong electron capture capability so that negative ions can be produced. Examples of gases that can create electronegative plasma include oxygen, fluorine, and chlorine.

The Bohm criterion says that ions can enter the sheath and reach the surface if their speed is higher than or equal to a certain speed designated as ion acoustic speed. Understanding of the Bohm criterion helps us to determine the conditions under which ions can effectively interact with the surfaces in plasma-based material processes. It is important in applications such as plasma etching, where ions are used to modify materials surface properties, and it helps us to optimize such processes. Mathematically, the Bohm criterion can be expressed as:

$$U_0 \geq C_P$$

where, $C_P = \sqrt{(K_B T_e)/M_P}$ is the ion acoustic speed with T_e as electron temperature and M_P as mass of the positive ions. If the ions are with velocities below the Bohm criterion, then they will be reflected into the plasma, and the surface remains shielded from the ion bombardment.

Researchers have successfully optimized the parameters for plasma nitriding by growing thin films of titanium using DC sputtering on the substrate of the glass. These films are then subjected to nitriding in a plasma system produced by hot cathode arc discharge [1, 2]. Scientists have successfully generated Co-like and Ni-like X-rays by transmitting laser-induced tin plasmas. The highest conversion efficiency of X-rays reached 3.54% when the power density was 5×10^{12} Wcm^{-2}, covering a range of 2π steradian [3]. Scientists have utilized oxygen and nitrogen plasmas to improve the surface of Poly methyl methacrylate (PMMA) polymer [4, 5]. Abe et al. [6] have explored the applications of isotropic etching, reactive ion etching (RIE), and plasma etching/cleaning techniques.

During these interactions, a layer called sheath is formed on the surface of the material. This sheath is greatly influenced by the presence of negative ions [7, 8]. In order to generate negatively charged particles, nitrogen gas has been used as an electronegative gas in a discharge process. The negative ions presence has a noticeable impact on this process [9]. In a different type of plasma called cylindrical DC glow discharge plasma, it has been observed that the plasma potential, electron temperature, and floating potential exhibit significant differences between constant current mode and constant pressure mode. In this context, the electron density of the plasma plays a crucial role in determining these differences [10]. Researchers have conducted an analysis to determine the sheath thickness formed on the surface of conducting spherical probe [11]. When space vehicles travel at supersonic speeds, the formation of a sheath also occurs on their surfaces [12, 13] and also in thruster devices [14]. In space propulsion devices such as magnetic nozzle, a separation of plasma species leads to acceleration of ions where concepts such as controlled divergence [15], detachment of plasma [16], enhancement of thrust [17] and role of density and pressure gradients as obtained in sheaths [18] are important. In simpler terms, such concepts are helpful in optimizing the propulsion performance. In space propulsion devices, the plasma used for propulsion is often unstable due to variations in plasma density and magnetic field across the system [19, 20]. This instability can also be observed in other types of plasmas with a cross-field configuration [21]. The concept of sheath formation is not limited to specific plasma systems [22–24]. It has also been applied in other plasma systems, such as microwave-generated plasma. In these systems, the instability is primarily caused by the energetic ions [25]. In electronegative plasmas like CF_4, O_2, and C_{60} plasmas, the sheath plays a significant role. As a result, the thickness of the sheath becomes an important factor to consider in these plasma systems [11, 26, 27].

The negative ions presence in various situations has been found to cause distinct changes in the plasma parameters. These changes in plasma parameters have been observed and studied in different contexts [7, 26–34]. In several theoretical models, the distribution of negative ions has been described by fluid behavior [26, 27, 30] whereas in some studies negative ions are employing Boltzmann distribution [7, 28, 29, 31–33]. These behaviors are entirely depending upon the choice of plasma parameters [35].

In macroscopic equilibrium states, the Maxwellian distribution for electrons has been observed to be valid. However, in certain plasma systems, the long-range interactions cannot be adequately described by the Maxwellian distribution. The population of electrons in such systems, as observed in theoretical investigations and space plasma observations, deviates from their thermodynamic equilibrium [36, 37]. When it comes to the gravitational and plasma systems, which involve long-range interactions, the Boltzmann statistics fail to provide an accurate description both theoretically and experimentally. To address this issue, a new statistical framework has been proposed by Tsallis [38]. This new statistics, known as Tsallis statistics, offers an alternative approach for the better understanding of such complex systems. Non-extensive statistics, based on non-extensive entropy, is a statistical framework that has been developed to accurately describe systems with particle distributions that deviate from the Maxwellian distribution. This framework, proposed by Tsallis [38], introduces a parameter q to account for the non-extensive behavior observed in these systems. The non-extensive statistics can also be applied to positive and negative ions to investigate dust acoustic double layers in opposite polarity dusty plasma. The non-extensivity of ions influences the behaviour of dust acoustic double layers [39].

Considering the previous research conducted by other scientists in related fields, this work primarily focuses on the plasma-surface interactions for the case of constant mean free path. To ensure a comprehensive analysis, we have taken into account certain imperative factors such as the ion-neutral collisions, and temperature of all species in a three-component plasma where both positive and negative ions are being described by fluid behavior whereas electrons are described by non-extensive statistics. The plasma sheath profile has been investigated for the very first time using this combination of charged species distribution.

2. Mathematical model

2.1 Continuity equation

2.1.1 For positive ions:

$$\nabla \cdot \mathbf{J} + \frac{\partial \rho}{\partial t} = 0 \tag{1}$$

where J is the current density and ρ is the charge density. Since we are considering steady state sheath, therefore $\partial\rho/\partial t = 0$. The Eq. (1) yields

$$\nabla \cdot \mathbf{J} = 0 \tag{2}$$

$$\nabla \cdot (nev) = 0 \tag{3}$$

$$\frac{\partial n_P v_P}{\partial x} = 0 \tag{4}$$

Here n_P and v_P are the density and velocity of the positive ions, respectively. Using $N_P = n_P/n_{P0}$, $U_P = v_P/C_{SP}$, and

$\xi = x/\lambda_{de}$ with N_P as normalised density of positive ions, n_{P0} as density of positive ions in plasma, U_P as normalized velocity of the positive ions, C_{SP} as sound velocity of positive ions, λ_{de} as Debye length, ξ as normalized distance and x as un-normalized distance from the sheath edge. Eq. (4) will read as follows.

$$\frac{\partial}{\partial \xi}(N_P U_P) = 0 \tag{5}$$

Now integrate above equation from sheath edge (ξ_0) to the probe position (ξ_P), we get

$$N_P = \frac{U_{P0} N_P}{U_P} \tag{6}$$

where N_{P0} and U_{P0} are density of positive ions in the plasma and velocity of the positive ions at the sheath edge, respectively.

2.1.2 For negative ions:

$$\frac{\partial n_N v_N}{\partial x} = 0 \tag{7}$$

where n_N and v_N are density and velocity of the negative ions. Using $N_N = n_N/n_{N0}$, $U_N = V_N/C_{SP}$, $\xi = x/\lambda_{de}$ with N_N as normalised density of the negative ions, n_{N0} as density of the negative ions in the plasma and U_N as velocity of the negative ions.

$$\frac{\partial}{\partial \xi}(N_N U_N) = 0$$

Now integrate above equation from sheath (ξ_0) to the probe position (ξ_P), we get

$$N_N = \frac{U_{N0} N_{N0}}{U_N} \tag{8}$$

where N_{N0} and U_{N0} are density of negative ions in the plasma and velocity of the negative ions at the sheath edge, respectively.

2.2 Momentum transfer equation

2.2.1 For positive ions:

$M_P[\partial v_P/\partial t + (\mathbf{v}_P \cdot \boldsymbol{\nabla})v_P]$ = force due to electric field + force due to thermal motion + force due to collisions

$$M_P[\frac{\partial v_P}{\partial t} + (\mathbf{v}_P \cdot \boldsymbol{\nabla})v_P] = Z_P e E - \frac{1}{n_P}\nabla P_P - M_P v_P \upsilon$$

where $\nabla P_P = k_B T_P(\partial n_P/\partial x$ is pressure gradient term, $\upsilon = n_g \sigma v_P$ is collisional frequency term, Z_P is charge on the positive ions, M_P is positive ion mass, and T_P is positive ion temperature.

$$M_P v_P \frac{\partial v_P}{\partial x} = -Z_P e \frac{\partial \Phi}{\partial x} - \frac{1}{n_P}\left(k_B T_P \frac{\partial n_P}{\partial x}\right) - M_P v_P (n_g \sigma v_P) \tag{9}$$

where n_g is neutral density, Φ is electric potential, and $\sigma = \{\sigma_s (v_P/C_{SP})^{\gamma}\} v_P$ is momentum transfer collisional cross section with σ_s as momentum transfer collisional cross-section at ion sound speed. Here, γ is a dimension-less parameter, taking values -1 to 0.

$$M_P v_P \frac{\partial v_P}{\partial x} = -Z_P e \frac{\partial \Phi}{\partial x} - \frac{1}{n_P} K_B T_P \frac{\partial n_P}{\partial x} - M_P n_g \sigma_s \frac{(v_P)^{\gamma+2}}{C_{SP}^{\gamma}} \tag{10}$$

We are interested to investigate the case of constant mean free path, therefore $\gamma = -1$ has been adopted in further calculations. Momentum transfer equations appear as follows.

$$M_P v_P \frac{\partial v_P}{\partial x} = -Z_P e \frac{\partial \Phi}{\partial x} - M_P n_g \sigma_s \frac{v_P}{C_{SP}^{-1}} - \frac{K_B T_P}{n_P}\frac{\partial n_p}{\partial x} \tag{11}$$

Using $N_P = n_P/n_{P0}$, $U_P = v_P/C_{sP}$, $\eta = -e\Phi/(K_B T_e)$, $\alpha = n_g \sigma_s \lambda_{de}$ and $\xi = x/\lambda_{de}$ in Eq. (11), we get

$$\frac{M_P U_P C_{SP}^2}{\lambda_{de}}\frac{\partial U_P}{\partial \xi} = \frac{Z_P K_B T_e}{\lambda_{de}}\frac{\partial \eta}{\partial \xi} - M_P \frac{\alpha U_P C_{SP}^2}{\lambda_{de}} - \frac{K_B T_e}{N_P}\frac{\gamma_P}{\lambda_{de}}\acute{N}_P$$

here $T_P/T_e = \gamma_P$ denotes the temperature ratio of positive ions to electrons. η is normalized electric potential and α is collisional parameter. Using relation $\acute{N}_P = -(N_P \acute{U}_P)/U_P$, we get

$$\frac{dU_P}{d\xi} = \left(1 + \frac{\gamma_P}{U_P^2}\right)^{-1}\left(\frac{Z_P}{U_P}\frac{\partial \eta}{\partial \xi} - \alpha\right) \tag{12}$$

2.2.2 For negative ions:

$$M_N v_N \frac{\partial v_N}{\partial x} = Z_N e \frac{\partial \Phi}{\partial x} - M_N n_g \sigma_s \frac{v_N}{C_{SP}^{-1}} - \frac{K_B T_N}{n_N}\frac{\partial n_N}{\partial x} \tag{13}$$

Using $U_N = v_N/C_{SP}$, $\eta = -e\Phi/(K_B T_e)$, $N_N = n_N/n_{N0}$, $\alpha = n_g \sigma_s \lambda_{de}$ and $\xi = x/\lambda_{de}$ in Eq. (13), we get

$$\frac{M_N U_N C_{SP}^2}{\lambda_{de}}\frac{\partial U_N}{\partial \xi} = -\frac{Z_N K_B T_e}{\lambda_{de}}\frac{\partial \eta}{\partial \xi} - M_N \frac{\alpha}{\lambda_{de}} U_N C_{SP}^2 + \frac{K_B T_N}{N_N}\frac{\gamma_N}{\lambda_{de}}\frac{N_N \acute{U}_N}{U_N}$$

Using $T_N/T_e = \gamma_N$ denotes the temperature ratio of negative ions to electrons. Using relation $\acute{N}_N = (N_N \acute{U}_N)/U_N$, we get

$$\frac{\partial U_N}{\partial \xi} = \left(1 - \frac{M_P}{U_N^2 M_N}\gamma_N\right)^{-1}\left[-\frac{Z_N}{U_N}\frac{M_P}{M_N}\frac{\partial \eta}{\partial \xi} - \alpha\right] \tag{14}$$

2.3 Poisson equation

$$\nabla^2 \Phi = -\frac{\rho}{\varepsilon_0} \tag{15}$$

$$\frac{\partial^2 \Phi}{\partial x^2} = -\frac{e}{\varepsilon_0}[Z_P n_P - Z_N n_N - n_e] \tag{16}$$

Using $N_P = n_P/n_{P0}$, $\eta = -e\Phi/(K_B T_e)$, $N_N = n_N/n_{N0}$, $N_e = n_e/n_{e0}$ with n_{N0} and n_{e0} as background negative ion density and electron density, respectively, we get

$$\frac{\partial^2 \eta}{\partial \xi^2} = Z_P \frac{U_{P0} N_{P0}^2}{U_P} - Z_N \frac{U_{P0} N_{N0}^2}{U_N} - N_e \tag{17}$$

here, N_{P0} and N_{N0}, respectively, are normalized electro-positivity and electro-negativity.

2.4 Non-extensive statistics

Using non-extensive statistics, the distribution of electrons can be written as follows.

$$n_e = n_{e0}\left[1+(q-1)\frac{e\Phi}{K_B T_e}\right]^{\frac{q+1}{2(q+1)}} \tag{18}$$

In normalized form, electron density will be read as follows.

$$N_e = \left[1-\eta(q-1)\right]^{\frac{q+1}{2(q+1)}} \tag{19}$$

3. Boundary conditions

The aforesaid differential equations are coupled in terms of U_P, U_N, and η. Therefore, a numerical method must be employed to solve these coupled equations. In the present work, Runge-Kutta (RK) method of fourth order which employed routine ODE-45 in MATLAB has been adopted. There are some more numerical methods to solve such non-linear equations that have proved to be significant in other areas of research as well [40–43]. In the given problem, to apply RK method initial values of positive and negative ions' velocity, electric potential, and electric field must be specified. Electronegativity, finite temperature of charged species, i.e., electrons, positive ions and negative ions are the other imperative parameters requisite for the solution of coupled equations. At $\xi = 10^{-3}$ or 10^{-4}, the point of plasma-sheath boundary or sheath edge has been considered. The magnitude of electric field and electric potential are 0.1 and 10^{-3}, respectively, at the sheath edge. $U_{P0} = 1$ and $U_{N0} = -1$ have been employed at the sheath edge [26, 27]. The quasi-neutrality holds perfectly at the sheath edge. The point, where floating wall condition is attained, will correspond to the probe position. Consequently, the distance between the points of attainment of floating wall condition and quasi-neutrality condition correspond to the sheath thickness. $\xi > 0$ is the sheath regime, whereas $\xi < 0$ is the plasma regime.

4. Results and discussions

4.1 Impact of electronegativity

Negative ions density plays a crucial role in the process of sheath formation, therefore, in this section, we have investigated the impact of electronegativity (N_{N0}) on several imperative plasma parameters like electric potential (η), positive ion density (N_P), and net space charge density (N_{net}).

The impact of N_{N0} on η has been depicted in Fig. 1. The quasi-neutrality holds perfectly at the sheath edge. The point, where floating wall condition is attained, will correspond to the probe position. Consequently, the distance between the points of attainment of floating wall condition and quasi-neutrality condition correspondence to the sheath thickness. When the system's electronegativity increases with a constant negative ion temperature, then having more negative ions near the sheath edge causes the starting point of quasi-neutrality conditions to move closer to the wall's surface. This means that for a denser background of negative ions, a smaller sheath magnitude is observed.

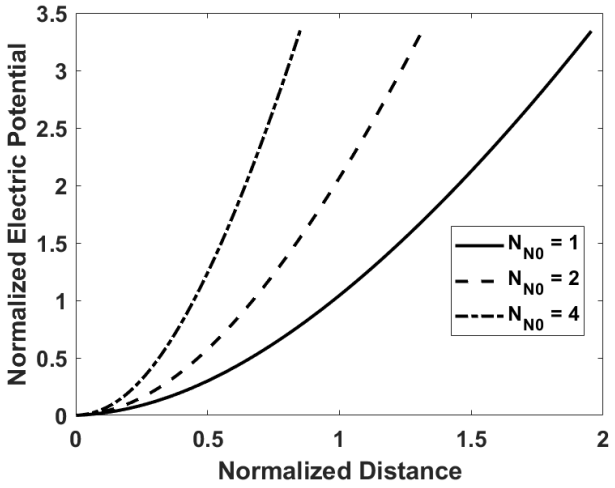

Figure 1. Impact of electronegativity (N_{N0}) on normalized electric potential (η) when $M_N/M_P = 0.275$, $\gamma = -1$, $\gamma_P = 0.1$, $\gamma_N = 0.1$, $\acute{\eta}_0 = 0.1$, $U_{P0} = 1$, $U_{N0} = -1$, $\alpha = 0.05$, $q = 0.25$, $Z_N = 1$, and $Z_P = 1$.

η at the wall or probe surface is not significantly changed by different N_{N0} because of a strong retarding force within the sheath for negative species. In sheath regime, therefore, η rises quickly for higher N_{N0}. Consequently, for higher N_{N0}, higher potential values are observed as we move from the sheath edge towards the wall or probe surface.

The impact of N_{N0} on U_P has been shown in Fig. 2. When the electronegativity increases, there is a steeper change in the electric potential, which results in stronger potential gradient. Consequently, acceleration experienced by the positive ions in the sheath region is increased considerably. Hence, when the electronegativity is higher, positive ions gain speed quickly in the sheath regime.

The impact of N_{N0} on N_{net} has been depicted in Fig. 3. N_{Net} is defined as the difference between the densities of positive species and negative species, i.e., $N_{Net} = N_P - N_N - N_e$.

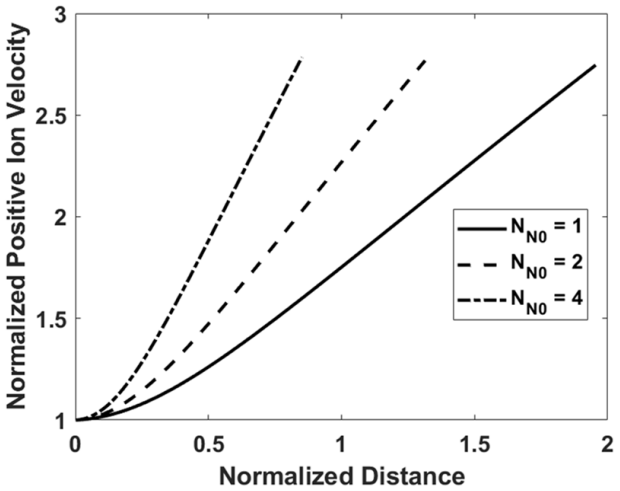

Figure 2. Impact of electronegativity (N_{N0}) on normalized positive ion velocity (U_P) when $M_N/M_P = 0.275$, $\gamma = -1$, $\gamma_P = 0.1$, $\gamma_N = 0.1$, $\acute{\eta}_0 = 0.1$, $U_{P0} = 1$, $U_{N0} = -1$, $\alpha = 0.05$, $q = 0.25$, $Z_N = 1$, and $Z_P = 1$.

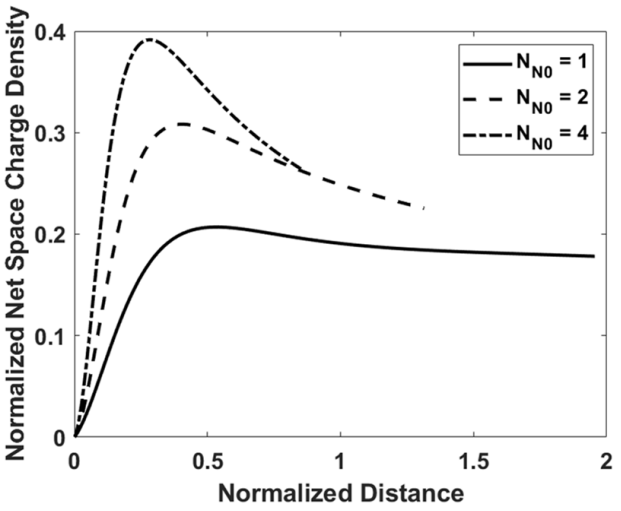

Figure 3. Impact of electronegativity (N_{N0}) on net space charge density (N_{net}) when $M_N/M_P = 0.275$, $\gamma = -1$, $\gamma_P = 0.1$, $\gamma_N = 0.1$, $\acute{\eta}_0 = 0.1$, $U_{P0} = 1$, $U_{N0} = -1$, $\alpha = 0.05$, $q = 0.25$, $Z_N = 1$, and $Z_P = 1$.

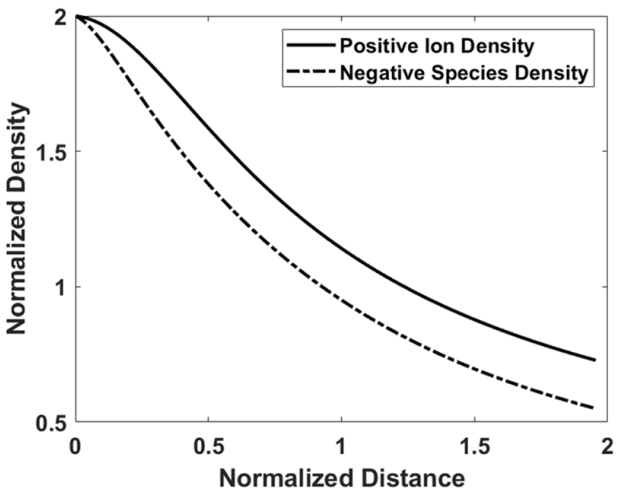

Figure 4. Impact of electronegativity (N_{N0}) on normalized density (N) when $M_N/M_P = 0.275$, $\gamma = -1$, $\gamma_P = 0.1$, $\gamma_N = 0.1$, $\acute{\eta}_0 = 0.1$, $U_{P0} = 1$, $U_{N0} = -1$, $\alpha = 0.05$, $q = 0.25$, $Z_N = 1$, and $Z_P = 1$.

The profile of N_{Net} is requisite to investigate so that the real nature of sheath formed can be analyzed. If N_{Net} is positive, then positive ions will form a sheath, and if N_{Net} is negative, then negative species will form a sheath. In our present model, a positive N_{Net} is obtained, confirming the formation of a sheath of positive ions only.

Since stronger potential gradient is recorded for higher electronegativity, de-acceleration (acceleration) experienced by the negative species (positive ions) in the sheath region is increased considerably. Consequently, a decreased (increased) density of negative species (positive ions) in the sheath region will be observed. With the increase (decrease) in positive ion density (negative species density), N_{Net} also goes up.

Impact of N_{N0} on normalized density (N) has been shown in Fig. 4. One can clearly see that density of positive species is much more than that of negative species throughout the sheath regime which confirms the formation of sheath of majority of positive ions. Here, solid line portrays the positive ion density whereas dashed line portrays the negative species density.

4.2 Impact of positive ion temperature

The influence of γ_P on the plasma sheath profile is imperative to analyse while dealing with plasma-surface interaction problems. This is due to the fact that positive ions' temperature imposed on material surface may lead to considerable alterations in its surface properties. Therefore, the choice of material and their sustainability is important to investigate [44–47]. Impact of γ_P on η has been depicted in Fig. 5. There are two kinds of forces:

Electrostatic force: These forces are arisen because of the negative potential at the probe, which pushes the charge particles in a specific direction.

Thermal force: This force happens because of finite temperature of charged species, making them move around randomly.

When the temperature of positive ions goes up, their random movement dominates over movement in a specific direction. Consequently, the number of positive ions reaches in sheath regime get reduced and as a result, the magnitude of η increases with a minimal rate.

The impact of γ_P on N_P has also been entertained herewith and portrayed in Fig. 6. When γ_P is higher, the electric potential changes with a minimal rate. This smooth change in potential leads to a smaller potential gradient. Additionally, the positive ions move around more randomly as their temperature rises. As a result, fewer positive ions are able to reach the sheath region. So, when γ_P is increased, the number of positive ions that can enter the sheath region reduces owing their relatively enhanced random movement. With increasing γ_P, an enhanced sheath thickness magnitude has been recorded. It has been seen that sheath thickness

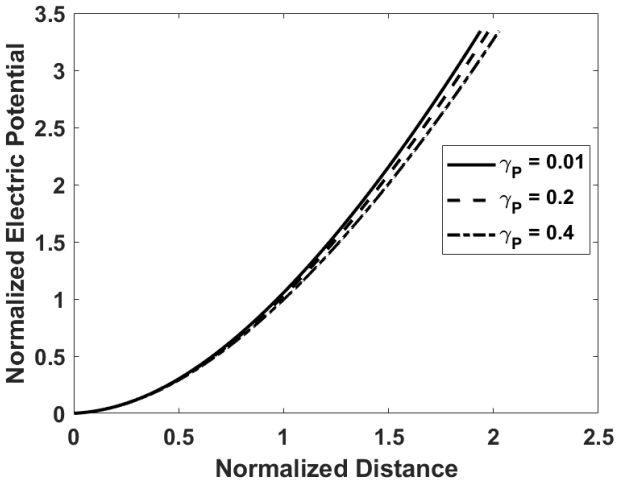

Figure 5. Impact of positive ion temperature (γ_P) on normalized electric potential (η) when $M_N/M_P = 0.275$, $\gamma = -1$, $\gamma_P = 0.1$, $\gamma_N = 0.1$, $\acute{\eta}_0 = 0.1$, $U_{P0} = 1$, $U_{N0} = -1$, $\alpha = 0.05$, $q = 0.25$, $Z_N = 1$, and $Z_P = 1$.

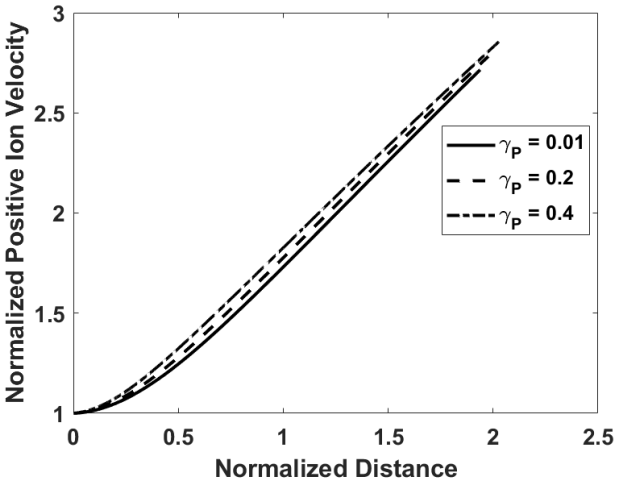

Figure 6. Impact of positive ion temperature (γ_P) on normalized positive ion density (N_P) when $M_N/M_P = 0.275$, $\gamma = -1$, $\gamma_P = 0.1$, $\gamma_N = 0.1$, $\acute{\eta}_0 = 0.1$, $U_{P0} = 1$, $U_{N0} = -1$, $\alpha = 0.05$, $q = 0.25$, $Z_N = 1$, and $Z_P = 1$.

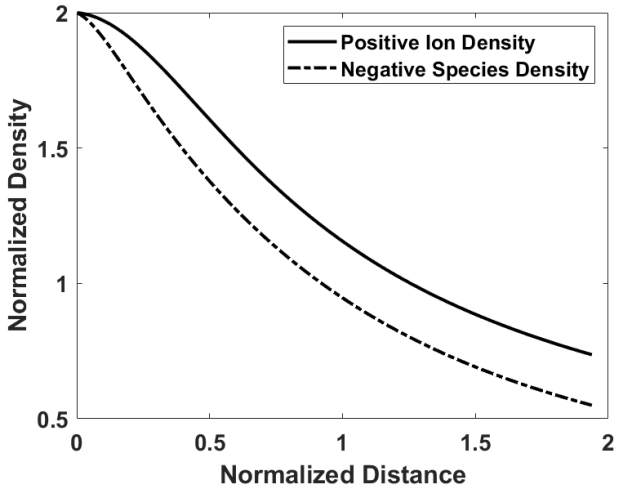

Figure 8. . Impact of positive ion temperature (γ_P) on normalized density (N) when $M_N/M_P = 0.275$, $\gamma = -1$, $\gamma_P = 0.1$, $\gamma_N = 0.1$, $\acute{\eta}_0 = 0.1$, $U_{P0} = 1$, $U_{N0} = -1$, $\alpha = 0.05$, $q = 0.25$, $Z_N = 1$, and $Z_P = 1$.

magnitude increases from 1.91 to 2.023 when γ_P increases from 0.01 to 0.4.

The impact of γ_P on N_{net} has been shown in Fig. 7. When γ_P increases, ions start to move around more randomly. This increased randomness means that fewer positive ions can make their way into the sheath regime. When positive ions are fewer in the sheath then N_{net} decreases. It is like the positive ions are less able to gather there because of their energetic movements caused by their higher temperature.

Impact of γ_P on normalized density (N) has been shown in Fig. 8. In the sheath, there are immense positive ions in comparison with that of negative species. This means that the sheath is mostly made up of the positive ions majorly. The positive ions are the dominant ones in this region.

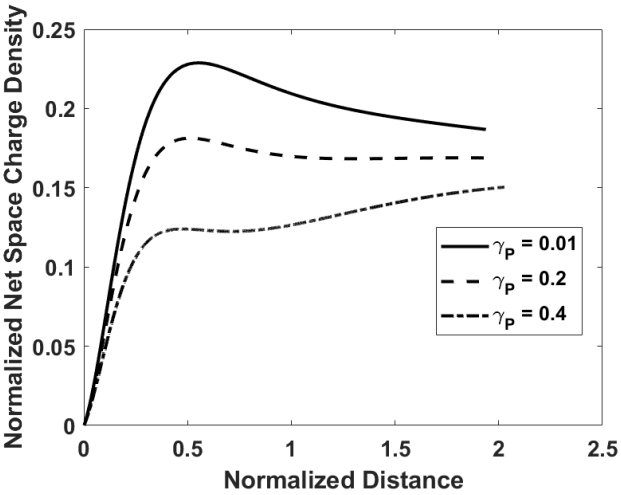

Figure 7. Impact of positive ion temperature (γ_P) on net space charge density (N_{net}) when $M_N/M_P = 0.275$, $\gamma = -1$, $\gamma_P = 0.1$, $\gamma_N = 0.1$, $\acute{\eta}_0 = 0.1$, $U_{P0} = 1$, $U_{N0} = -1$, $\alpha = 0.05$, $q = 0.25$, $Z_N = 1$, and $Z_P = 1$.

5. Conclusion

From the present work, we can conclude that increasing electronegativity results in relatively higher acceleration for the positive ions, electric potential profile shows abrupt increment, reduced sheath thickness, and higher net charge density. Higher positive ions temperature results in lesser potential gradient profile and smaller net space charge density owing increased randomness in positive ions motion. Also, higher magnitude sheath thickness is reported for higher positive ions temperature.

Higher potential gradients are favoured in plasma-based material processing [48] because they lead to improved thin-film development since positive ions are collecting in a relatively smaller area.

Ethical Approval

This manuscript does not report on or involve the use of any animal or human data or tissue. So the ethical approval is not applicable.

Authors Contributions

The author contribution of this article contribute is as follows: Rajat Dhawan, Conceptualization, Investigation, Methodology, Software, Supervision, Validation, Writing – review & editing; Sarika, Formal Analysis, Methodology, Writing–original draft; Rajeev Sehrawat, Data Curation, Formal Analysis; Rashmi Mittal, Visualization, Data Curation; Ishan Choudhary, Data Curation, Formal analysis.

Availability of Data and Materials

The data that support the findings of this study are available from the corresponding author upon

reasonable request.

Conflict of Interests
The authors declare that they have no known competing financial interests or personal relationships that could have appeared to influence the work reported in this paper.

References

[1] O. Singh, H. K. Malik, R. P. Dahiya, and P. Kumar. "Influence of negative bias voltage on structural and mechanical properties of nanocrystalline TiNx thin films treated in hot cathode arc discharge plasma system.". *Ceram. Int.*, **42**:18019–18024, 2016. DOI: https://doi.org/10.1016/j.ceramint.2016.08.032.

[2] O. Singh, P. Dahiya, H. K. Malik, P. Kumar, and V. Singh. "Investigation of titanium nitride thin films treated in hot cathode arc discharge plasma system.". *Appl. Sci. Lett.*, **2**:37–41, 2016. DOI: https://doi.org/10.17571/appslett.2016.02006.

[3] B. Atalay, R. Aydin, A. Demir, N. Kenar, and E. Kacar. "Simulation of Ni-like and Co-like X-rays emitted from laser produced tin plasmas. ". *Czechoslov. J. Phys.*, **56**:B430–B435, 2006. DOI: https://doi.org/10.1007/s10582-006-0234-z.

[4] D. Dorranian, Z. Abedini, A. Hojabri, and M. Ghoranneviss. "Structural and optical characterization of PMMA surface treated in low power nitrogen and oxygen RF plasmas.". *J. Non-Oxide Glas.*, **1**:217–229, 2009.

[5] M. Jafari and D. Dorranian. "Surface modification of PMMA polymer in the interaction with oxygen-argon RF plasma.". *J. Theor. Appl. Phys.*, **5**:59–66, 2011.

[6] H. Abe, M. Yoneda, and N. Fujiwara. "Developments of plasma etching technology for fabricating semiconductor devices.". *Jpn. J. Appl. Phys.*, **47**:1435–1455, 2008. DOI: https://doi.org/10.1143/JJAP.47.1435.

[7] R. Dhawan and H. K. Malik. "Sheath formation mechanism in collisional electronegative warm plasma with two-temperature non-extensive distributed electrons and ionization. ". *J. Appl. Phys.*, **133**, 2023. DOI: https://doi.org/10.1063/5.0120616.

[8] R. Dhawan and H. K. Malik. "Are the oscillations found in magnetized collisional electronegative warm plasma artifact during plasma-surface interaction? ". *J. Phys. D. Appl. Phys.*, **56**:485206, 2023. DOI: https://doi.org/10.1088/1361-6463/acf228.

[9] F. Araghi and D. Dorranian. "Effect of negative ions on the characteristics of plasma in a cylindrical discharge.". *J. Theor. Appl. Phys.*, **7**:41, 2013. DOI: https://doi.org/10.1186/2251-7235-7-41.

[10] D. Dorranian and M. Alizadeh. "Effect of negative oxygen ions on the characteristics of plasma in a cylindrical DC discharge.". *J. Theor. Appl. Phys.*, **8**:122, 2014. DOI: https://doi.org/10.1007/s40094-014-0122-z.

[11] H. K. Malik and R. Dhawan. "Sheath structure in electronegative plasma having cold ions: An impact of negative ions' mass.". *IEEE Trans. Plasma Sci.*, **48**:2408–2417, 2020. DOI: https://doi.org/10.1109/TPS.2020.2998717.

[12] L. Malik, S. Rawat, M. Kumar, and A. Tevatia. "Simulation studies on aerodynamic features of Eurofighter Typhoon and Dassault Rafale combat aircraft. ". *Mater. Today Proc.*, **38**:191–197, 2021. DOI: https://doi.org/10.1016/j.matpr.2020.06.536.

[13] L. Malik and A. Tevatia. "Comparative analysis of aerodynamic characteristics of F16 and F22 combat aircraft using computational fluid dynamics.". *Def. Sci. J.*, **71**, 2021. DOI: https://doi.org/10.14429/dsj.71.15762.

[14] A. Aanesland, D. Rafalskyi, J. Bredin, P. Grondein, N. Oudini, P. Chabert, D. Levko, L. Garrigues, and G. Hagelaar. "The PEGASES gridded ion-ion thruster performance and predictions.". *IEEE Trans. Plasma Sci.*, **43**:321–326, 2015. DOI: https://doi.org/10.1109/TPS.2014.2369534.

[15] L. Malik, M. Kumar, and I. V. Singh. "A three-coil setup for controlled divergence in magnetic nozzle.". *IEEE Trans. Plasma Sci.*, **49**:2227–2237, 2021. DOI: https://doi.org/10.1109/TPS.2021.3090457.

[16] L. Malik. "Tapered coils system for space propulsion with enhanced thrust: A concept of plasma detachment.". *Propuls. Power Res.*, **11**:171–180, 2022. DOI: https://doi.org/10.1016/j.jppr.2022.04.002.

[17] L. Malik. "Novel concept of tailorable magnetic field and electron pressure distribution in a magnetic nozzle for effective space propulsion. ". *Propuls. Power Res.*, **12**:59–68, 2023. DOI: https://doi.org/10.1016/j.jppr.2023.02.002.

[18] L. Malik. "In-flight plume control and thrust tuning in magnetic nozzle using tapered-coils system under the effect of density gradient. ". *IEEE Trans. Plasma Sci.*, **51**:1325–1333, 2023. DOI: https://doi.org/10.1109/TPS.2023.3263009.

[19] H. K. Malik, J. Tyagi, and D. Sharma. "Growth of Rayleigh instability in a Hall thruster channel having dust in exit region.". *AIP Adv.*, **9**:55220, 2019. DOI: https://doi.org/10.1063/1.5050688.

[20] S. Singh and H. K. Malik. "Role of ionization and electron drift velocity profile to Rayleigh instability in a Hall thruster plasma.". *J. Appl. Phys.*, **112**:13307, 2012. DOI: https://doi.org/10.1063/1.4733339.

[21] Munish, R. Dhawan, R. Kumar, and H. K. Malik. "Density gradient driven instability in an plasma system having temperature gradients.". *J. Taibah Univ. Sci.*, **16**:725–731, 2022. DOI: https://doi.org/10.1080/16583655.2022.2108303.

[22] S. Kumar, V. Dhaka, D. K. Singh, and H. K. Malik. "Analytical approach for the use of different gauges in bubble wakefield acceleration.". *J. Theor. Appl. Phys.*, **15**:1–12, 2021. DOI: https://doi.org/10.30495/jtap.152102].

[23] S. Kumar, D. K. Singh, and H. K. Malik. "Numerical investigations of electron-self-injection in different shaped bubbles in wakefield acceleration. ". *J. Theor. Appl. Phys.*, **17**, 2023. DOI: https://doi.org/10.57647/J.JTAP.2023.1702.21.

[24] S. Kumar, D. K. Singh, and H. K. Malik. "Comparative study of ultrashort single-pulse and multi-pulse driven laser wakefield acceleration. ". *Laser Phys. Lett.*, **20**:26001, 2022. DOI: https://doi.org/10.1088/1612-202X/aca978.

[25] M. Starodubtsev, M. Kamal-Al-Hassan, H. Ito, N. Yugami, and Y. Nishida. "Low-frequency sheath instability in a non-Maxwellian plasma with energetic ions. ". *Phys. Rev. Lett.*, **92**:45003, 2004. DOI: https://doi.org/10.1103/PhysRevLett.92.045003.

[26] R. Dhawan and H. K. Malik. "Sheath formation criterion in collisional electronegative warm plasma. ". *Vacuum*, **177**:109354, 2020. DOI: https://doi.org/10.1016/j.vacuum.2020.109354.

[27] R. Dhawan and H. K. Malik. "Sheath Characteristics in Plasma carrying Finite Mass Negative Ions and Ionization at Low Frequency. ". *Chinese J. Phys.*, **66**:560–572, 2020. DOI: https://doi.org/10.1016/j.cjph.2020.06.007.

[28] K. Yasserian, M. Aslaninejad, M. Borghei, and M. Eshghabadi. "Electronegative plasma-sheath characteristics over a wide range of collisionality.". *J. Theor. Appl. Phys.*, **4**:26–29, 2010.

[29] R. Moulick, M. K. Mahanta, and K. S. Goswami. "Effect of collision parameters in electronegative plasma sheath with two species of positive ions.". *Phys. Plasmas.*, **20**:94501, 2013. DOI: https://doi.org/10.1063/1.4820803.

[30] R. Dhawan and H. K. Malik. "Behaviour of sheath in electronegative warm plasma. ". *J. Theor. Appl. Phys.*, **14**:121–128, 2020. DOI: https://doi.org/10.1007/s40094-020-00369-2.

[31] R. Dhawan and H. K. Malik. "Modelling of electronegative collisional warm plasma for plasma-surface interaction process.". *Plasma Sci. Technol.*, **23**: 45402, 2021. DOI: https://doi.org/10.1088/2058-6272/abeb03.

[32] J. Li, J. X. Ma, and Z. Wei. "Sheath and boundary conditions in a collisional magnetized warm electronegative plasma.". *Phys. Plasmas.*, **20**:63503, 2013. DOI: https://doi.org/10.1063/1.4811479.

[33] K. Yasserian and M. Aslaninejad. "On the space-charge formation in a collisional magnetized electronegative plasma.". *Plasmas*, **19**:73507, 2012. DOI: https://doi.org/10.1063/1.4736861.

[34] R. Dhawan, M. Malik, and H. K. Malik. "Modified Bohm's criterion in a collisional electronegative plasma having two-temperature non-extensive electrons. ". *J. Theor. Appl. Phys.*, **16**:1–8, 2022. DOI: https://doi.org/10.30495/jtap.162240.

[35] R. Dhawan, M. Kumar, and H. K. Malik. "Influence of ionization on sheath structure in electropositive warm plasma carrying two-temperature electrons with non-extensive distribution.". *Phys. Plasmas*, **27**:63515, 2020. DOI: https://doi.org/10.1063/5.0003242.

[36] H. R. Pakzad. "Ion acoustic solitary waves in plasma with nonthermal electron and positron. ". *Phys. Lett. A.*, **373**:847–850, 2009. DOI: https://doi.org/10.1016/j.physleta.2008.12.066.

[37] W. Stöber, A. Fink, and E. Bohn. "Ion acoustic solitons and double layers in electron–positron–ion plasmas with dust particulates.". *Astrophys. Space Sci.*, **314**:121–127, 2008. DOI: https://doi.org/10.1007/s10509-008-9748-0.

[38] C. Tsallis. "Possible generalization of Boltzmann-Gibbs statistics. ". *J. Stat. Phys.*, **52**:479–487, 1988. DOI: https://doi.org/10.1007/BF01016429.

[39] N. Mirghassemzadeh, D. Dorranian, and S. Saviz. "Influence of ions nonextensivity on the dynamics of dust acoustic double layers in a magnetized self-gravitating dusty plasma. ". *Waves in Random and Complex Media*, :1–16, 2022. DOI: https://doi.org/10.1080/17455030.2022.2065041.

[40] L. Malik and A. Escarguel. "Role of the temporal profile of femtosecond lasers of two different colours in holography. ". *Europhysics Lett. (EPL)*, **124**:64002, 2019. DOI: https://doi.org/10.1209/0295-5075/124/64002.

[41] L. Malik. "Dark hollow lasers may be better candidates for holography.". *Opt. Laser Technol.*, **132**:106485, 2020. DOI: https://doi.org/10.1016/j.optlastec.2020.106485.

[42] L. Malik, A. Escarguel, M. Kumar, A. Tevatia, and R. S. Sirohi. "Uncovering the remarkable contribution of lasers peak intensity region in holography. ". *Laser Phys. Lett.*, **18**:86003, 2021. DOI: https://doi.org/10.1088/1612-202X/ac0bc4.

[43] L. Malik. "Towards designing a lockable self-folding origami. ". *Master's Thesis, Princeton Univ., NJ*, , 2024.

[44] L. Malik, G. S. Saini, M. Malik, and A. Tevatia. "Sustainability of wind turbine blade: instantaneous real-time prediction of its failure using machine learning and solution based on materials and design.". *Handbook of Sustainable Materials: Modelling, Characterization, and Optimization. CRC Press*, :399–430, 2023. DOI: https://doi.org/10.1201/9781003297772.

[45] R. Dhawan, H. K. Malik, and D. Dorranian. "Applications of sustainable materials.". *Handbook of Sustainable Materials: Modelling, Characterization, and Optimization. CRC Press*, :301–322, 2023. DOI: https://doi.org/10.1201/9781003297772-16.

[46] L. Malik, G. S. Saini, and A. Tevatia. "A self-sustained machine learning model to predict the in-flight mechanical properties of a rocket nozzle by inputting material properties and environmental conditions.". *Handbook of Sustainable Materials: Modelling, Characterization, and Optimization. CRC Press*, :431–456, 2023. DOI: https://doi.org/10.1201/9781003297772-21.

[47] R. Dhawan, H. K. Malik, and A. Kumar. "Sustainability of materials: concepts, history, and future.". *Handbook of Sustainable Materials: Modelling, Characterization, and Optimization. CRC Press*, :93–110, 2023. DOI: https://doi.org/10.1201/9781003297772-6.

[48] H. K. Malik. "Laser-Matter Interaction for Radiation and Energy. 1st Ed.". *Boca Raton, CRC Press*, , 2021. DOI: https://doi.org/10.1201/b21799.